

Double-degenerate Bose-Fermi mixture of strontium and lithium

Zhu-Xiong Ye¹, Li-Yang Xie¹, Zhen Guo¹, Xiao-Bin Ma¹, Gao-Ren Wang², Li You^{1,3}, and Meng Khoon Tey^{1,3,*}

¹State Key Laboratory of Low-Dimensional Quantum Physics, Department of Physics, Tsinghua University, Beijing 100084, China

²School of Physics, Dalian University of Technology, Dalian 116024, China

³Frontier Science Center for Quantum Information, Beijing, China

 (Received 28 June 2020; accepted 11 August 2020; published 8 September 2020)

We report on the attainment of a degenerate Fermi gas of ${}^6\text{Li}$ in contact with a Bose-Einstein condensate (BEC) of ${}^{84}\text{Sr}$. A degeneracy of $T/T_F = 0.33(3)$ is observed with 1.6×10^5 ${}^6\text{Li}$ atoms in the two lowest-energy hyperfine states together with an almost pure BEC of 3.1×10^5 ${}^{84}\text{Sr}$ atoms. The elastic s -wave scattering length between ${}^6\text{Li}$ and ${}^{84}\text{Sr}$ is estimated to be $|a_{6\text{Li}-84\text{Sr}}| = (7.1_{-1.7}^{+2.6})a_0$ (a_0 is the Bohr radius) from measured interspecies thermalization rates in an optical dipole trap.

DOI: [10.1103/PhysRevA.102.033307](https://doi.org/10.1103/PhysRevA.102.033307)

I. INTRODUCTION

Ultracold-gas mixtures composed of different species provide a useful platform to study few- and many-body physics, including the BEC-BCS crossover [1,2], Efimov state [3–5], and crystalline quantum phase [6]. They are also ideal starting points to prepare heteronuclear ground-state molecules [7,8], which hold great promise for the study of ultracold chemical reactions [9,10], quantum computation and simulation [11,12], and precision measurement [13]. In addition, large mass mismatch gas mixtures can also be used to study impurity in superfluids [14,15], mass imbalanced Cooper pairs [16–19], and heteronuclear trimer states [20,21]. Previously, quantum degenerate mixtures of alkali-metal atoms have been the main powerhouse for such studies.

In recent years, mixtures of alkali-metal and alkaline-earth(-like) atoms have attracted much attention. Significant progress has been made in both theory [22–38] and experiment [39–50]. In particular, Feshbach resonances in RbSr [51] and LiYb [52] have been observed, paving the way to produce ground-state group-I+group-II molecules. One of the motivations to produce such molecules is that they possess a magnetic dipole moment on top of an electric dipole moment. This property makes such molecules good candidates for studies of lattice-spin models [53], collective spin excitations in optical lattice [54], and precision measurements of, for example, the electric-dipole moment (EDM) of the electron [55] and proton-to-electron mass ratio [36]. So far, mixtures of alkali-metal and alkaline-earth(-like) atoms which have been cooled down to quantum degeneracy include Li-Yb [39,40], Rb-Yb [41], Rb-Sr [42], and Cs-Yb [43].

In this work, we report the production of a quantum degenerate mixture composed of alkali-metal ${}^6\text{Li}$ and alkaline-earth-metal ${}^{84}\text{Sr}$ in a far-off-resonant optical dipole trap. Previously, we estimated the s -wave scattering length between ${}^{88}\text{Sr}$ and ${}^6\text{Li}$ atoms to be $|a_{6\text{Li}-88\text{Sr}}| = (14.4_{-3.2}^{+4.9})a_0$ from measurement of the interspecies thermalization rates [56]. Earlier

experience seems to disfavor this number as too small to support efficient sympathetic cooling for typical conditions near quantum degeneracy, which typically requires good elastic s -wave scattering length of the order of $100a_0$ instead. Moreover, changing the ${}^{88}\text{Sr}$ to other isotopes is not expected to substantially change the ${}^6\text{Li}$ -Sr scattering. This is because ${}^6\text{Li}$ is much lighter than strontium; changing ${}^{88}\text{Sr}$ to ${}^{84}\text{Sr}$, for example, changes the ${}^6\text{Li}$ - ${}^x\text{Sr}$ reduced mass by merely 0.3%. Since the ground-state molecular potential of Li-Sr can only support roughly 23 vibrational bound states [22,23], a 0.3% variation in the reduced mass would hardly have any impact on the overall energy structure of the Li-Sr molecules, and thus the interspecies scattering length. Our simulation based on the potential from [22] predicts a change of only a few a_0 in the ${}^6\text{Li}$ -Sr scattering length from ${}^{88}\text{Sr}$ to ${}^{84}\text{Sr}$. Indeed, based on the same measurement method detailed in Ref. [56], we estimate $|a_{6\text{Li}-84\text{Sr}}|$ to be $(7.1_{-1.7}^{+2.6})a_0$.

Even though changing to the ${}^{84}\text{Sr}$ isotope does not result in a more favorable interspecies thermalization, it is more useful for our present goal of realizing a double degenerate mixture of Li and Sr. This is because ${}^{84}\text{Sr}$, which has an s -wave scattering length of $a_{84\text{Sr}-84\text{Sr}} = 123a_0$, can be readily cooled by evaporation to quantum degeneracy by itself [57,58], in contrast to ${}^{88}\text{Sr}$ with $a_{88\text{Sr}-88\text{Sr}} = -2a_0$. On the other hand, due to the lack of efficient sympathetic cooling, the ${}^6\text{Li}$ gas, in a mixture of its two lowest hyperfine sublevels, must also be able to support rapid thermalization by itself for efficient evaporative cooling. As the ${}^6\text{Li}$ atoms in the two lowest hyperfine sublevels do not interact at zero magnetic field, we choose to perform evaporation of the ${}^{84}\text{Sr}$ - ${}^6\text{Li}$ mixture at a magnetic field of 330 G. At this field, the s -wave scattering length between the two lowest hyperfine substates of ${}^6\text{Li}$ is $a_{12} = -290a_0$. This field, however, is not expected to have much effect on the Sr-Sr and Sr-Li scattering lengths since the ground state of bosonic Sr has no magnetic dipole moment and thus does not couple with various spins of ${}^6\text{Li}$ unless higher-order couplings are included [37,51].

In short, our strategy towards a double degenerate Li and Sr mixture is to employ a Sr isotope and a magnetic field that would allow efficient evaporative cooling of individual

*mengkhoon_tey@tsinghua.edu.cn

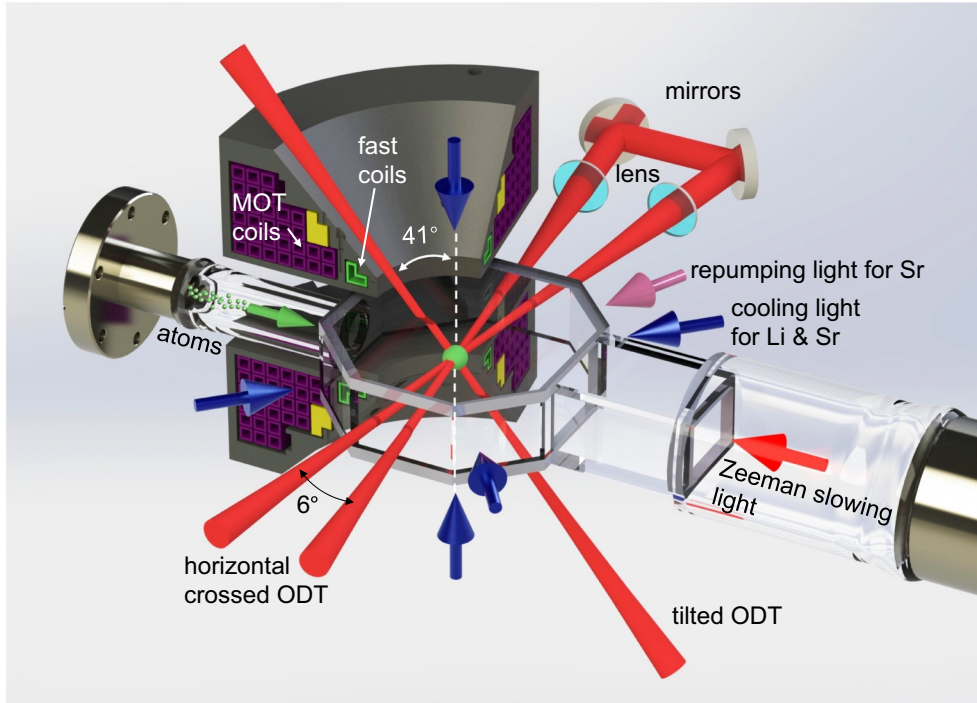


FIG. 1. Illustration of the experimental setup. The main science chamber is an octagonal glass cell. Overlapped cooling light beams for both species are represented by the blue arrows [59]. The ${}^6\text{Li} + {}^{84}\text{Sr}$ atomic beams (green arrow) are overlapped and copropagating, as are their corresponding Zeeman slowing light beams (red arrow). The MOT coils and the “fast” coils can operate in either Helmholtz or anti-Helmholtz configurations to provide bias magnetic fields and magnetic field gradients. The far-off-resonant 1064 nm crossed optical dipole trap (CODT) for both species is formed at the common crossing of two horizontal beams and a beam tilted at 41° to the vertical axis [60].

species. At the end of evaporation, we obtain Fermi degenerate ${}^6\text{Li}$ with 8.2×10^4 atoms in each spin at $T/T_F = 0.33(3)$, in contact with an almost pure Bose-Einstein condensate (BEC) of ${}^{84}\text{Sr}$ with 3.1×10^5 atoms.

This article is organized as follows: Section II describes the main experiment setup and how we sequentially load ${}^6\text{Li}$, and then ${}^{84}\text{Sr}$, into a 1064 nm optical dipole trap (ODT). Section III discusses the evaporation cooling procedure as well as the evidence for the double degenerate Bose-Fermi mixture. The properties of the mixture over the evaporation are analyzed and discussed in Sec. IV. Section V concludes the article.

II. PREPARING ${}^{84}\text{Sr}$ AND ${}^6\text{Li}$ ATOMS IN OPTICAL DIPOLE TRAP

Figure 1 illustrates the heart of our setup, which has been described in detail in Ref. [56]. In brief, overlapped light beams for cooling both lithium and strontium are indicated by blue arrows [59]. Copropagating ${}^6\text{Li} + {}^{84}\text{Sr}$ atomic beams and their corresponding Zeeman slowing beams are represented by a green arrow and a red arrow, respectively. The far-off-resonant crossed optical trap (CODT) for both species is constructed by crossing three 1064 nm light beams (red beams) at their respective waists: two horizontal beams crossing at 6° have a common waist of $32 \mu\text{m}$, and the other is tilted at 41° to the vertical axis and has a waist of $54 \mu\text{m}$ [60].

As the magnetic field gradients for optimal loading and cooling of the lithium and strontium differ significantly, we

sequentially (1) load the ${}^6\text{Li}$ magneto-optical trap (MOT), perform gray-molasses cooling, and then transfer ${}^6\text{Li}$ atoms into the horizontal crossed optical dipole trap (HCODT); (2) load the ${}^{84}\text{Sr}$ 461 nm “blue” MOT, cool ${}^{84}\text{Sr}$ atoms using the 689 nm “red” MOT, and transfer them into the same HCODT; (3) evaporatively cool both ${}^6\text{Li}$ and ${}^{84}\text{Sr}$ into quantum degeneracy at a bias magnetic field of 330 G by reducing the trap depth. The sequence of our experiment is detailed in Fig. 2.

In more detail, the experiment starts with magneto-optical trapping of ${}^6\text{Li}$ atoms using cooling and repumping light locked to the $671 \text{ nm } {}^2S_{1/2} \rightarrow {}^2P_{3/2}$ (D2) transitions and a magnetic field gradient of 21.4 G/cm. A cloud of 1.6×10^8 atoms is accumulated with a temperature $\sim 3 \text{ mK}$ after 3 s. The MOT is then compressed (CMOT) by ramping the magnetic field gradient to 37.5 G/cm (and changing the powers and detuning of the cooling and repumping light simultaneously; see Fig. 2) in 3 ms. This process reduces the gas temperature to $\sim 690 \mu\text{K}$. To further cool and increase the phase-space density of the atomic cloud, we apply the gray-molasses (GM) cooling technique [61]. The GM can only work efficiently when the magnetic field is smaller than 0.1 G. Due to the induction of the MOT coils, however, the residual magnetic field at the cloud takes 1.1 ms to drop below 0.1 G. But a lithium atom is relatively light, and a 1.1 ms free expansion of the lithium cloud would greatly reduce the loading efficiency into the HCODT. As a remedy, a second set of coils, called “fast coils,” in a Helmholtz configuration dynamically compensates for the residual magnetic field from the MOT coils (see Fig. 2), reducing the free-expansion time from

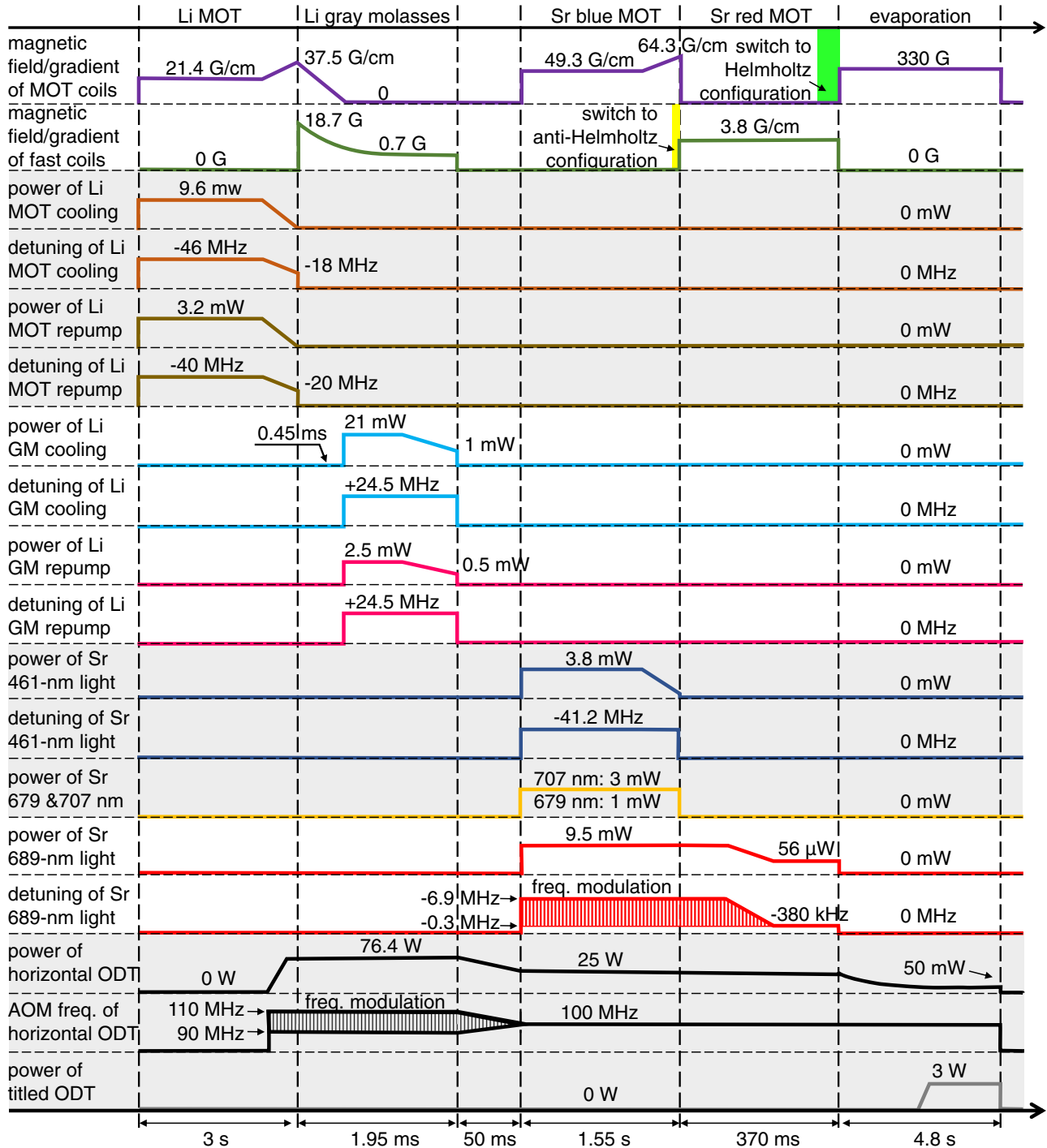


FIG. 2. Schematic for main controls and timings for our experiment procedure. The reported powers of the various MOT beams are those of a single beam. Each MOT beam has a waist of ~ 6 mm.

1.1 to 0.45 ms. After 1.5 ms of GM cooling, a cloud with 1×10^8 atoms at $\sim 50 \mu\text{K}$ is obtained. As the $2S_{1/2}|F = 1/2\rangle \rightarrow 2P_{1/2}|F' = 3/2\rangle$ repumping light is switched off 0.1 ms earlier than $2S_{1/2}|F = 3/2\rangle \rightarrow 2P_{1/2}|F' = 3/2\rangle$ cooling light at the end of the GM, atoms are equally distributed in the $|F = 1/2, m_F = \pm 1/2\rangle$ states.

Transfer of the ${}^6\text{Li}$ atoms into the HCODT (without the 41° -tilted beam) happens concurrently with the GM process. To improve loading efficiency, the trapping volume of the HCODT is enlarged by ~ 4 – 5 times at the beginning of

the GM. This is done by modulating the frequency of the radio frequency (rf) applied to the acousto-optic modulator (AOM) which diffracts the horizontal ODT beam, from 90 to 110 MHz, at a modulating frequency of 2.6 MHz. The modulation amplitude is reduced linearly to 0 in 50 ms after the GM process (Fig. 2). Meanwhile, the power of the HCODT beam is reduced linearly from 76.4 to 25 W, stopping at a HCODT depth of $k_B \times 1.9$ mK (k_B is the Boltzmann constant) for ${}^6\text{Li}$. At the end of the GM stage, about 3.3×10^6 atoms are loaded into the HCODT at a temperature of $\sim 300 \mu\text{K}$.

While the ${}^6\text{Li}$ atoms are trapped in the HCODT, Zeeman-slowed ${}^{84}\text{Sr}$ atoms are cooled and captured in a “blue” MOT operating on a 461 nm light, red detuned from the $5s^2\,{}^1S_0 - 5s5p\,{}^1P_1$ transition by 41.2 MHz, at a magnetic field gradient of 49.3 G/cm. As weak leak from the cooling cycle populates the $5s5p\,{}^3P_2$ metastable state at this stage [57], two repumping light beams at 679 and 707 nm (pink arrow in Fig. 1) are shone onto the blue MOT to bring these atoms back into the cooling cycle. After 1.5 s loading, the ${}^{84}\text{Sr}$ atom cloud is compressed by increasing the magnetic field gradient to 64.3 G/cm within 50 ms. Meanwhile, the power of each 461 nm beam is decreased from 3.8 to 0.2 mW. At the end of the blue MOT stage, about 4.5×10^7 ${}^{84}\text{Sr}$ atoms at a temperature of ~ 2 mK are collected.

Further cooling of the ${}^{84}\text{Sr}$ atoms is achieved in a “red” MOT operating on the 7.5-kHz-linewidth ${}^1S_0 - {}^3P_1$ transition at 689 nm, at a magnetic field gradient of 3.8 G/cm. To increase the capturing velocity of the red MOT, we frequency modulate the light, producing a detuning ranging from -6.9 MHz to -300 kHz with a spacing of 50 kHz. After a 75 ms modulation cooling period (which ensures that almost all atoms are captured from the blue MOT into the red MOT), the cloud is compressed by ramping down the frequency modulation within 145 ms, ending with a single-frequency MOT at a detuning of -380 kHz (see Fig. 2). At the same time, the power of each 689 nm beam is reduced from 9.5 mW to $56\ \mu\text{W}$. The single-frequency MOT is then operated for another 150 ms to further cool down the atoms. More than 2.1×10^7 atoms at a temperature $3.4\ \mu\text{K}$ are obtained at the end of the red MOT stage.

Loading of the ${}^{84}\text{Sr}$ atoms into the HCODT occurs at the single-frequency red MOT stage. In order to achieve efficient loading, we optimize the overlap between the HCODT and the single-frequency red MOT by adjusting the bias magnetic fields. During the whole Sr-MOT stages, the power of HCODT is held constant at 25 W, corresponding to a trap depth of $k_B \times 1.7$ mK for strontium. Note that operation of the Sr blue MOT would result in a loss of the ${}^6\text{Li}$ atoms in the HCODT, presumably due to light-assisted collision loss [62]. We adjust the loading times for each species to obtain a favorable ratio in the atom numbers for subsequent evaporative cooling. With a 1.5 s blue MOT loading, we obtain 1.2×10^6 ${}^6\text{Li}$ atoms and 1.2×10^7 ${}^{84}\text{Sr}$ atoms in the HCODT at a common temperature of $\sim 180\ \mu\text{K}$ after thermalization for 500 ms between the two species.

III. EVAPORATION TO A DOUBLE DEGENERATE MIXTURE

For an optical trap from 1064 nm light, the ratios of trap depth and trap frequency for ${}^6\text{Li}$ vs ${}^{84}\text{Sr}$ are $U_{6\text{Li}}/U_{84\text{Sr}} = 1.1$ and $\omega_{6\text{Li}}/\omega_{84\text{Sr}} = 3.9$, respectively. The almost-equal depth for Li and Sr is useful for keeping the temperatures of Li and Sr nearly the same in the early stage of the evaporation despite weak interspecies interactions since the temperature of a gas is typically about 1/10 of the U/k_B after adequate evaporation (see Ref. [63] and Sec. IV).

Forced evaporation of the mixture starts by reducing the power of HCODT roughly exponentially from 25 W to 50 mW in 4.8 s. After 1.5 s into the forced evaporation,

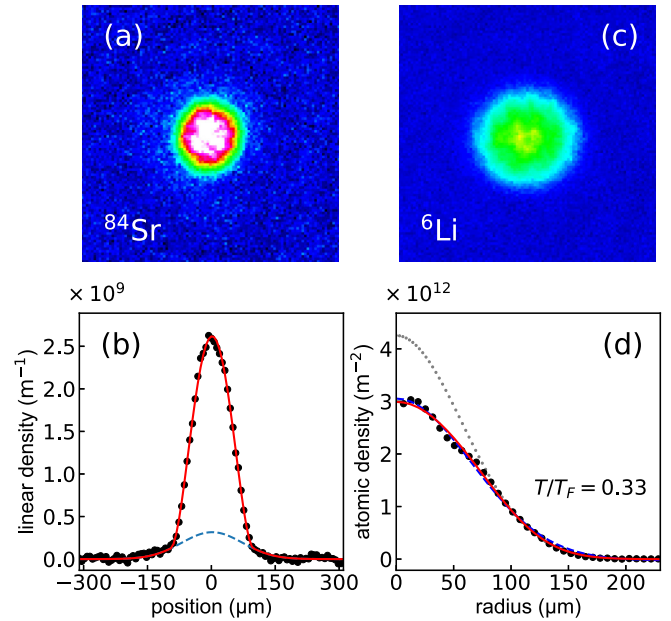


FIG. 3. Evidence of quantum degenerate Bose ${}^{84}\text{Sr}$ and Fermi ${}^6\text{Li}$ gases. (a) Absorption image of a BEC of ${}^{84}\text{Sr}$, 22 ms after releasing from the trap. (b) Integrated density profiles of (a). The red solid line represents a fit with a bimodal distribution, while the blue dashed line denotes a Gaussian fit to the thermal part. (c) Absorption image of a quantum degenerate ${}^6\text{Li}$ Fermi gas, 2 ms after releasing from the trap. (d) The azimuthally averaged density distribution of the ${}^6\text{Li}$ Fermi gas, averaged over 10 measurements. A fit using Eq. (1) (solid red line) deviates slightly from a Gaussian (dashed blue line). If we fit only the outer thermal wing (gray dotted line), outside the disk with a radius $\sqrt{2}w$ (where w is the $1/e$ width of a Gaussian fit to the full distribution), the deviation becomes even more evident.

the power of the 41° -tilted ODT is raised linearly from 0 to 3 W in 450 ms, and then held constant until the end of the evaporation (see Fig. 2). At the end of the evaporation, we obtain a Fermi-degenerate ${}^6\text{Li}$ gas with 8.2×10^4 atoms in each spin state at $T/T_F = 0.33(3)$, in contact with an almost pure BEC of ${}^{84}\text{Sr}$ with 3.1×10^5 atoms. At this moment, the CODT frequencies and depth are, respectively, $(\omega_x, \omega_y, \omega_z) = 2\pi \times (718, 720, 150)$ Hz and $k_B \times 5.6\ \mu\text{K}$ for Li, and $2\pi \times (144, 183, 37)$ Hz and $k_B \times 0.35\ \mu\text{K}$ for ${}^{84}\text{Sr}$, taking the gravitation sag into consideration.

As evidence for the double degeneracy, we show in Fig. 3 the absorption images and density profiles of the ${}^{84}\text{Sr}$ BEC and the Fermi-degenerate ${}^6\text{Li}$ gas after free expansion. The one-dimensional (1D) integrated density profile of the ${}^{84}\text{Sr}$ gas after a 22 ms time of flight [Fig. 3(b)] exhibits a textbook-like bimodal distribution, signifying a BEC in contact with a small thermal component at a temperature of 105(10) nK. To quantify the degeneracy of the ${}^6\text{Li}$ Fermi gas, we determine the ratio of temperature T to the Fermi temperature T_F by fitting the azimuthally averaged density profile of the ${}^6\text{Li}$ gas after a 2 ms time of flight [Fig. 3(d)] using [64]

$$n(r) = A \text{Li}_2\left(-\zeta e^{-\frac{r^2}{2\sigma^2}}\right). \quad (1)$$

Here, Li_n represents the n th-order polylogarithm function, and ρ is the radius from the center of the cloud. A , σ , and ζ are

fitting parameters. The width σ and fugacity ζ of the cloud can be used to extract $T = m\sigma^2/k_B t_{\text{tof}}^2$ (t_{tof} is the time of flight) and $T/T_F = [-6\text{Li}_3(-\zeta)]^{-1/3}$, respectively. The former gives degeneracy depth T/T_F , given that $T_F = \hbar\bar{\omega}(6N_\uparrow)^{1/3}/k_B$ [$\bar{\omega} = (\omega_x\omega_y\omega_z)^{1/3}$, and N_\uparrow is the number of atoms in one of the ${}^6\text{Li}$ spins]. The latter is used for a consistency check [65] for results from the former when $\zeta > 2$ (corresponding to $T/T_F < 0.46$). For Fig. 3(d), we obtain, from the former method, $T = 539(31)$ nK, $T_F = 1.62(10)$ μK , and thus $T/T_F = 0.33(3)$, which is consistent with $T/T_F = 0.31(4)$ from the latter method.

IV. PROPERTIES OF THE MIXTURE OVER THE EVAPORATION

In this section, we analyze properties of the mixture at different moments of the evaporation process. The temperatures and atom numbers of the gases are obtained from absorption images, taken at 330 G, after free expansion. Other properties of the gases are computed from these quantities in conjunction with the calibrated powers and beam widths of the trapping light beams.

Figure 4(a) plots the temperatures of the ${}^{84}\text{Sr}$ and ${}^6\text{Li}$ gases as a function of evaporation time. It shows that the temperatures of the two species are equal in the first 2 s of the evaporation, but deviate substantially towards the end of the process. This suggests that heat exchange between the two species is efficient initially, but diminishes at the later stage of the evaporation. Without sufficient interspecies thermalization, the temperature of each gas is mainly affected by their corresponding trap depths U [63]. This is evident by noticing the similarities in the curves for the temperatures (main figure) and the computed trap depths U (inset). As U is reduced by the gravity more strongly for the heavier ${}^{84}\text{Sr}$ than for the lighter ${}^6\text{Li}$, the ${}^{84}\text{Sr}$ gas gets much colder than the ${}^6\text{Li}$ one at the end of the evaporation. Figure 4(b) shows the ratios $k_B T/U$ for the respective gases over the evaporation time. For ${}^6\text{Li}$, $k_B T/U$ stays roughly at the level of 0.1 throughout the evaporation, getting slightly smaller over time. For ${}^{84}\text{Sr}$, this parameter increases from approximately 0.1 in the beginning to 0.26 in the end. Figure 4(c) displays phase-space densities (PSDs) of the gases versus atom numbers. Roughly speaking, both the ${}^{84}\text{Sr}$ and ${}^6\text{Li}$ gases gain about three orders of magnitude in the PSDs after losing one order of magnitude in the atom number, signifying rather efficient cooling. The PSD of ${}^6\text{Li}$ nevertheless levels off towards the end of the evaporation due to Fermi pressure of the gas. It should be noted that at the end of the evaporation, the gravity sags the center of the ${}^6\text{Li}$ (${}^{84}\text{Sr}$) cloud by ~ 0.5 μm (8.6 μm), while the Thomas-Fermi radius (assuming zero temperature) of ${}^6\text{Li}$ (${}^{84}\text{Sr}$) is ~ 14.8 μm (5.9 μm). This means that the two clouds remain fully overlapped until the very end of the evaporation process.

In Fig. 5, we show the interspecies and intraspecies thermal equilibrium time constants τ , defined as $\frac{1}{\tau} = -\frac{1}{\Delta T} \frac{d(\Delta T)}{dt}$ (ΔT is the temperature difference between two thermal components) [56,66], as a function of the evaporation time. The figure shows that the intraspecies thermalization time constants of ${}^{84}\text{Sr}$ and ${}^6\text{Li}$ remain below 10 ms throughout the evaporation. Such a value is small enough to guarantee good

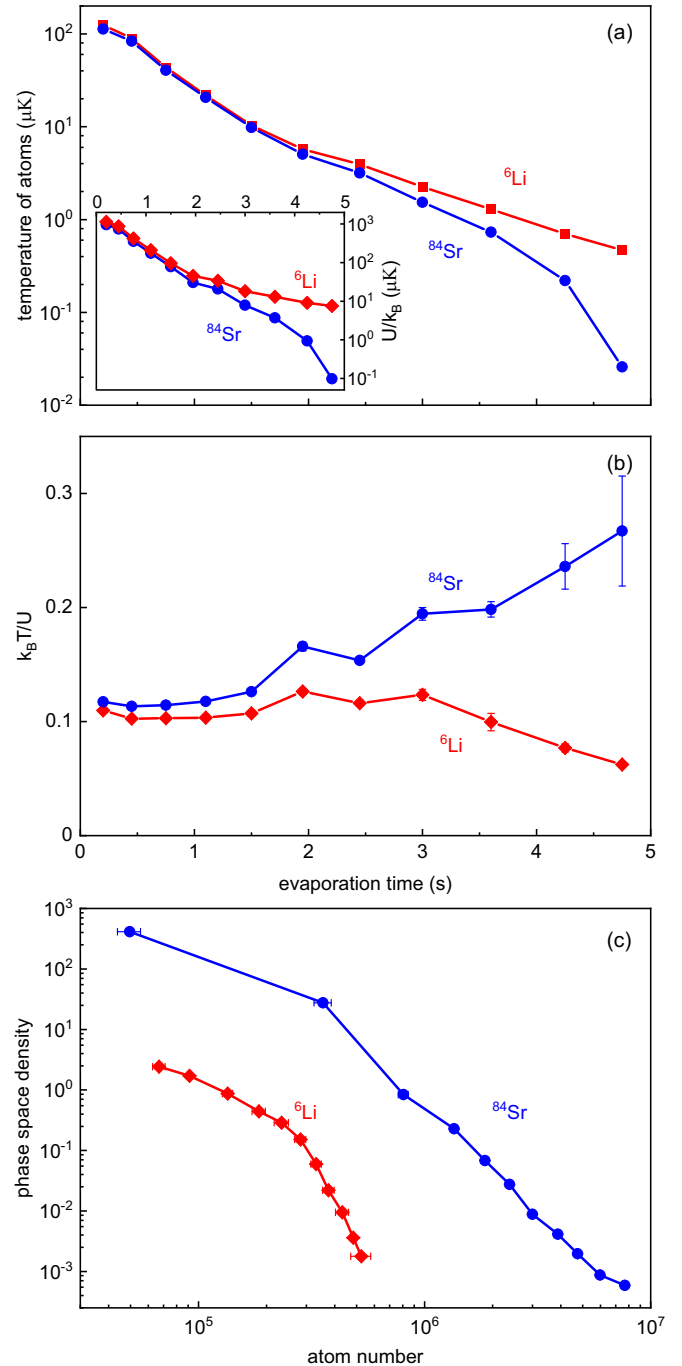


FIG. 4. Temperatures T , trap depths U , and phase-space densities at various stages of the evaporation process. (a) The temperatures of the ${}^6\text{Li}$ and ${}^{84}\text{Sr}$ gases show strong correlations with the respective depths of the ODT (inset), signifying insufficient interspecies thermalization towards the end of the evaporation. The error bars from five measurements are smaller than the symbols in this logarithmic-scale plot. (b) Ratios of average thermal energy $k_B T$ to the trap depth U . (c) Phase-space densities vs atom numbers. The PSD is defined as $n\lambda_T^3$, where n is the gas density at the center of the trap, and $\lambda_T = \sqrt{2\pi\hbar^2/mk_B T}$ is the thermal de Broglie wavelength. The atom number of ${}^6\text{Li}$ represents that of a single component.

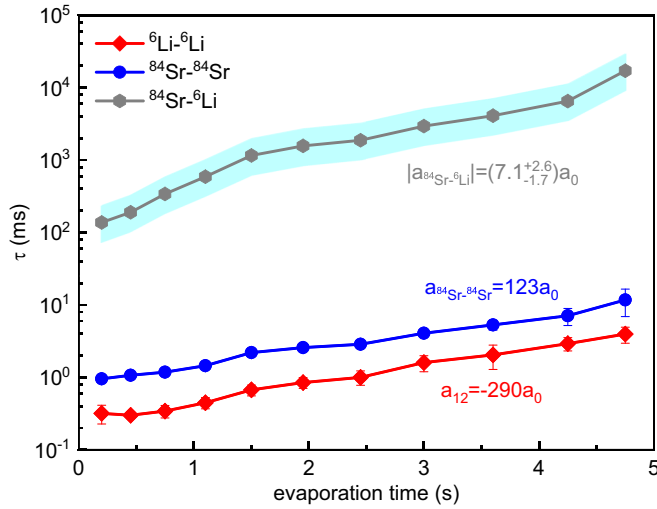


FIG. 5. The computed intraspecies and interspecies thermal equilibrium time constants τ of ${}^6\text{Li}$ and ${}^{84}\text{Sr}$ atoms during evaporation. The blue shaded region represents uncertainty arising from the uncertainty in the interspecies s -wave scattering length. The influence of quantum degeneracy to collision cross sections, which would have effects to the last few points, is ignored in this calculation.

intraspecies thermalization over the whole evaporation process, which lasts over a few seconds. On the other hand, the interspecies thermalization is two to three orders of magnitude slower due to a much smaller interspecies scattering cross section $\propto a_s^2$ (a_s is the s -wave scattering length). The interspecies thermalization time constant increases from 100 ms in the beginning to 10 s at the end of the evaporation. This supports the observation in Fig. 4, where the temperature difference between the two species grows over the evaporation process.

To see if the weak interspecies interactions play any role at all during the evaporative cooling process, we repeat the experiment without ${}^{84}\text{Sr}$ or without ${}^6\text{Li}$. For each scenario, we keep the initial numbers of ${}^6\text{Li}$ or ${}^{84}\text{Sr}$ atoms at the beginning of the evaporation the same as those of the mixture experiment. The results, which are shown in Fig. 6, clearly demonstrate that the presence of ${}^{84}\text{Sr}$ helps bringing the ${}^6\text{Li}$ Fermi gas into deeper degeneracy. The latter is achieved by increasing the number of ${}^6\text{Li}$ atoms at the expense of ${}^{84}\text{Sr}$ atoms for any given ODT power, a clear signature of sympathetic cooling. This phenomenon can be readily understood given that the trap depth of ${}^{84}\text{Sr}$ is always lower than that of ${}^6\text{Li}$.

V. CONCLUSION

In summary, we realize a quantum degenerate mixture of fermionic ${}^6\text{Li}$ and bosonic ${}^{84}\text{Sr}$ atoms in a crossed optical dipole trap, and determine the elastic s -wave scattering length between ${}^6\text{Li}$ and ${}^{84}\text{Sr}$ atoms to be $|a_{\text{Li-Sr}}| = (7.1^{+2.6}_{-1.7})a_0$ by measuring interspecies thermalization rates. Our results pave the way to studies including Li-Sr polar molecules and

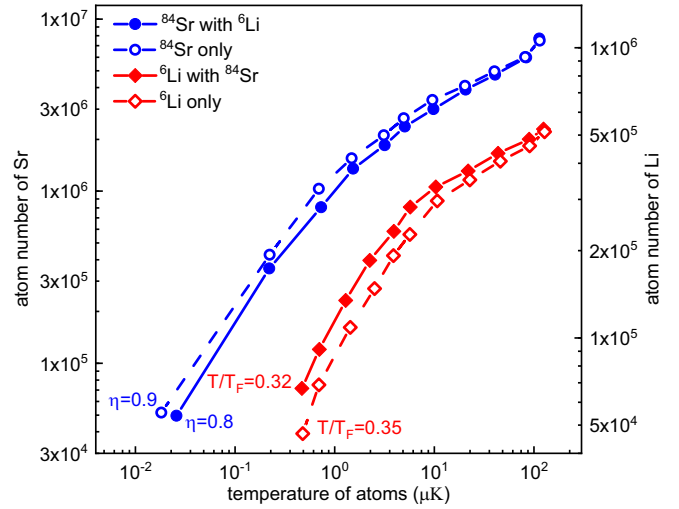


FIG. 6. Effects of sympathetic cooling. The presence of ${}^{84}\text{Sr}$ helps bringing the ${}^6\text{Li}$ Fermi gas into deeper degeneracy. $\eta = N_c/N$ represents the degeneracy of ${}^{84}\text{Sr}$, where N_c is the atom numbers in the condensate and N is the total atom number of the gas. Error bars are smaller than the symbols. The atom number of ${}^6\text{Li}$ represents that of a single component.

impurity superfluids. Further improvement for our experiment includes adding a gradient magnetic field to lower the trap depth for the ${}^6\text{Li}$ at the end of the evaporation process, so as to further reduce (increase) the temperature (quantum degeneracy) of the gas (we are not able to further reduce the power of the trapping light since this would result in spilling of the heavier ${}^{84}\text{Sr}$ at the moment).

We note in passing that we have also realized a double degenerate mixture of ${}^6\text{Li}$ and ${}^{84}\text{Sr}$ at zero magnetic field where there is no intraspecies ${}^6\text{Li}$ collisions. Here, the ${}^6\text{Li}$ gas can only be sympathetically cooled by the ${}^{84}\text{Sr}$ atoms. This process causes much more atom loss in both species compared to the evaporation reported above at 330 G. We realize a degenerate ${}^6\text{Li}$ Fermi gas at $T/T_F = 0.50(7)$ with total atom number of $N_{\text{Li}} = 4.9 \times 10^4$, coexisting with a ${}^{84}\text{Sr}$ BEC of 2.1×10^5 atoms in this case. In the future, we plan to probe the binding energy spectrum of near-dissociation Li-Sr molecules to determine the long-range dispersion coefficients of the ground-state molecular potential. Such information would be useful for producing ground-state molecules of Li-Sr.

ACKNOWLEDGMENTS

We thank Xibo Zhang for helpful discussions. This work is supported by the National Key Research and Development Program of China under Grant No. 2018YFA0306503, and the National Natural Science Foundation of China under Grants No. 91636213, No. 91736311, No. 11574177, No. 91836302, and No. 11654001, and Open Research Fund Program of the State Key Laboratory of Low-Dimensional Quantum Physics (Grant No. KF201802).

[1] I. Bloch, J. Dalibard, and W. Zwerger, *Rev. Mod. Phys.* **80**, 885 (2008).

[2] R. B. Diener and M. Randeria, *Phys. Rev. A* **81**, 033608 (2010).

- [3] J. Levinsen, T. G. Tiecke, J. T. M. Walraven, and D. S. Petrov, *Phys. Rev. Lett.* **103**, 153202 (2009).
- [4] G. Barontini, C. Weber, F. Rabatti, J. Catani, G. Thalhammer, M. Inguscio, and F. Minardi, *Phys. Rev. Lett.* **103**, 043201 (2009).
- [5] S.-K. Tung, K. Jiménez-García, J. Johansen, C. V. Parker, and C. Chin, *Phys. Rev. Lett.* **113**, 240402 (2014).
- [6] D. S. Petrov, G. E. Astrakharchik, D. J. Papoular, C. Salomon, and G. V. Shlyapnikov, *Phys. Rev. Lett.* **99**, 130407 (2007).
- [7] J. Deiglmayr, A. Grochola, M. Repp, K. Mörthbauer, C. Glück, J. Lange, O. Dulieu, R. Wester, and M. Weidemüller, *Phys. Rev. Lett.* **101**, 133004 (2008).
- [8] J. M. Sage, S. Sainis, T. Bergeman, and D. DeMille, *Phys. Rev. Lett.* **94**, 203001 (2005).
- [9] S. Ospelkaus, K. K. Ni, D. Wang, M. H. De Miranda, B. Neyenhuis, G. Quémener, P. S. Julienne, J. L. Bohn, D. S. Jin, and J. Ye, *Science* **327**, 853 (2010).
- [10] M.-G. Hu, Y. Liu, D. D. Grimes, Y.-W. Lin, A. H. Gheorghhe, R. Vexiau, N. Bouloufa-Maafa, O. Dulieu, T. Rosenband, and K.-K. Ni, *Science* **366**, 1111 (2019).
- [11] P. Rabl, D. DeMille, J. M. Doyle, M. D. Lukin, R. J. Schoelkopf, and P. Zoller, *Phys. Rev. Lett.* **97**, 033003 (2006).
- [12] D. DeMille, *Phys. Rev. Lett.* **88**, 067901 (2002).
- [13] L. D. Carr, D. DeMille, R. V. Krems, and J. Ye, *New J. Phys.* **11**, 055049 (2009).
- [14] K. Targońska and K. Sacha, *Phys. Rev. A* **82**, 033601 (2010).
- [15] F. M. Spiegelhalter, A. Trenkwalder, D. Naik, G. Hendl, F. Schreck, and R. Grimm, *Phys. Rev. Lett.* **103**, 223203 (2009).
- [16] A. Gezerlis, S. Gandolfi, K. E. Schmidt, and J. Carlson, *Phys. Rev. Lett.* **103**, 060403 (2009).
- [17] A. Trenkwalder, C. Kohstall, M. Zaccanti, D. Naik, A. I. Sidorov, F. Schreck, and R. Grimm, *Phys. Rev. Lett.* **106**, 115304 (2011).
- [18] S.-T. Wu, C.-H. Pao, and S.-K. Yip, *Phys. Rev. B* **74**, 224504 (2006).
- [19] M. Iskin, *Phys. Rev. A* **78**, 021604(R) (2008).
- [20] R. Pires, J. Ulmanis, S. Häfner, M. Repp, A. Arias, E. D. Kuhnle, and M. Weidemüller, *Phys. Rev. Lett.* **112**, 250404 (2014).
- [21] J. P. D’Incao and B. D. Esry, *Phys. Rev. A* **73**, 030702(R) (2006).
- [22] R. Guérout, M. Aymar, and O. Dulieu, *Phys. Rev. A* **82**, 042508 (2010).
- [23] G. Gopakumar, M. Abe, M. Hada, and M. Kajita, *J. Chem. Phys.* **138**, 194307 (2013).
- [24] J. Mitroy and M. W. J. Bromley, *Phys. Rev. A* **68**, 052714 (2003).
- [25] J. M. Standard and P. R. Certain, *J. Chem. Phys.* **83**, 3002 (1985).
- [26] J. F. Stanton, *Phys. Rev. A* **49**, 1698 (1994).
- [27] S. Kotochigova, A. Petrov, M. Linnik, J. Kos, and P. S. Julienne, *J. Chem. Phys.* **135**, 164108 (2011).
- [28] T. Chen, S. Zhu, X. Li, J. Qian, and Y. Wang, *Phys. Rev. A* **89**, 063402 (2014).
- [29] J. V. Pototschnig, A. W. Hauser, and W. E. Ernst, *Phys. Chem. Chem. Phys.* **18**, 5964 (2016).
- [30] L. Augustovičová and P. Soldán, *J. Chem. Phys.* **136**, 084311 (2012).
- [31] M. Tomza, *Phys. Rev. A* **88**, 012519 (2013).
- [32] S. Guo, M. Bajdich, L. Mitas, and P. J. Reynolds, *Molec. Phys.* **111**, 1744 (2013).
- [33] Q. Shao, L. Deng, X. Xing, D. Gou, X. Kuang, and H. Li, *J. Phys. Chem. A* **121**, 2187 (2017).
- [34] S. N. Tohme and M. Korek, *Chem. Phys. Lett.* **638**, 216 (2015).
- [35] A. Allouche and M. Aubert-Frécon, *Chem. Phys. Lett.* **222**, 524 (1994).
- [36] M. Kajita, G. Gopakumar, M. Abe, and M. Hada, *J. Phys. B: Atom. Molec. Opt. Phys.* **46**, 025001 (2012).
- [37] D. A. Brue and J. M. Hutson, *Phys. Rev. Lett.* **108**, 043201 (2012).
- [38] I. Zeid, T. Atallah, S. Kontar, W. Chmaisani, N. El-Kork, and M. Korek, *Comput. Theor. Chem.* **1126**, 16 (2018).
- [39] H. Hara, Y. Takasu, Y. Yamaoka, J. M. Doyle, and Y. Takahashi, *Phys. Rev. Lett.* **106**, 205304 (2011).
- [40] A. H. Hansen, A. Khramov, W. H. Dowd, A. O. Jamison, V. V. Ivanov, and S. Gupta, *Phys. Rev. A* **84**, 011606(R) (2011).
- [41] V. D. Vaidya, J. Tiamsuphat, S. L. Rolston, and J. V. Porto, *Phys. Rev. A* **92**, 043604 (2015).
- [42] B. Pasquiou, A. Bayerle, S. M. Tzanova, S. Stellmer, J. Szczepkowski, M. Parigger, R. Grimm, and F. Schreck, *Phys. Rev. A* **88**, 023601 (2013).
- [43] A. Guttridge, S. A. Hopkins, M. D. Frye, J. J. McFerran, J. M. Hutson, and S. L. Cornish, *Phys. Rev. A* **97**, 063414 (2018).
- [44] T. Aoki, Y. Yamanaka, M. Takeuchi, Y. Torii, and Y. Sakemi, *Phys. Rev. A* **87**, 063426 (2013).
- [45] C. Bruni and A. Görlitz, *Phys. Rev. A* **94**, 022503 (2016).
- [46] E. Schwanke, H. Knöckel, A. Stein, A. Pashov, S. Ospelkaus, and E. Tiemann, *J. Phys. B: Atom. Molec. Opt. Phys.* **50**, 235103 (2017).
- [47] S. Kraft, F. Vogt, O. Appel, F. Riehle, and U. Sterr, *Phys. Rev. Lett.* **103**, 130401 (2009).
- [48] F. Lackner, G. Krois, T. Buchsteiner, J. V. Pototschnig, and W. E. Ernst, *Phys. Rev. Lett.* **113**, 153001 (2014).
- [49] L. M. Russon, G. K. Rothschof, M. D. Morse, A. I. Boldyrev, and J. Simons, *J. Chem. Phys.* **109**, 6655 (1998).
- [50] J. D’Incao, C. Effantin, A. Bernard, G. Fabre, R. Stringat, A. Boulezhar, and J. Vergs, *J. Chem. Phys.* **100**, 945 (1994).
- [51] V. Barbé, A. Ciamei, B. Pasquiou, L. Reichsöllner, F. Schreck, P. S. Żuchowski, and J. M. Hutson, *Nat. Phys.* **14**, 881 (2018).
- [52] A. Green, H. Li, J. H. S. Toh, X. Tang, K. C. McCormick, M. Li, E. Tiesinga, S. Kotochigova, and S. Gupta, *Phys. Rev. X* **10**, 031037 (2020).
- [53] A. Micheli, G. K. Brennen, and P. Zoller, *Nat. Phys.* **2**, 341 (2006).
- [54] J. Pérez-Ríos, F. Herrera, and R. V. Krems, *New J. Phys.* **12**, 103007 (2010).
- [55] E. R. Meyer and J. L. Bohn, *Phys. Rev. A* **80**, 042508 (2009).
- [56] X.-B. Ma, Z.-X. Ye, L.-Y. Xie, Z. Guo, L. You, and M. K. Tey, *Chinese Phys. Lett.* **36**, 073401 (2019); *ibid.* **36**, 109902 (2019).
- [57] S. Stellmer, M. K. Tey, B. Huang, R. Grimm, and F. Schreck, *Phys. Rev. Lett.* **103**, 200401 (2009).
- [58] Y. N. Martínez de Escobar, P. G. Mickelson, M. Yan, B. J. DeSalvo, S. B. Nagel, and T. C. Killian, *Phys. Rev. Lett.* **103**, 200402 (2009).
- [59] The overlapped cooling light beams include 671 nm light (with four different frequencies) for realizing MOT and gray molasses of ${}^6\text{Li}$, and 461 and 671 nm light for realizing blue MOT and red MOT of ${}^{84}\text{Sr}$, respectively.

- [60] The polarizations of the horizontal beams are both linear but made orthogonal to each other to avoid interference. The 41° -tilted beam, which is derived from a different laser, interferes with the horizontal ones, but at a beating frequency too fast to cause heating.
- [61] A. Burchianti, G. Valtolina, J. A. Seman, E. Pace, M. De Pas, M. Inguscio, M. Zaccanti, and G. Roati, *Phys. Rev. A* **90**, 043408 (2014).
- [62] A. Gallagher and D. E. Pritchard, *Phys. Rev. Lett.* **63**, 957 (1989).
- [63] K. M. O'Hara, M. E. Gehm, S. R. Granade, and J. E. Thomas, *Phys. Rev. A* **64**, 051403(R) (2001).
- [64] This profile is a good approximation for a spatially integrated Fermi-Dirac distribution for a gas initially trapped in a harmonic potential and after a time of flight larger than the trap oscillation periods.
- [65] M. K. Tey, S. Stellmer, R. Grimm, and F. Schreck, *Phys. Rev. A* **82**, 011608(R) (2010).

- [66] We calculate the thermalization time constant τ using

$$\frac{1}{\tau} = -\frac{1}{\Delta T} \frac{d(\Delta T)}{dt} = \frac{\xi}{\alpha} \bar{n} \bar{v}. \quad (2)$$

Here, $\Delta T = T_1 - T_2$ is the temperature difference between thermal components 1 and 2. $\alpha = 2.7$ is the average times of collisions needed for thermalization between colliding pairs with equal mass [67], and $\xi = \frac{4m_1m_2}{(m_1+m_2)^2}$ is a correction factor to α for nonequal mass partners ($\xi = 0.249$ for ${}^6\text{Li} - {}^{84}\text{Sr}$ mixture). The mean relative velocity $\bar{v} = \sqrt{\frac{8k_B}{\pi} (\frac{T_1}{m_1} + \frac{T_2}{m_2})}$ and the overlap density $\bar{n} = (\frac{1}{N_1} + \frac{1}{N_2}) \int n_1(\mathbf{r})n_2(\mathbf{r})d^3r$, with

$$\int n_1(\mathbf{r})n_2(\mathbf{r})d^3r = \frac{N_1N_2(m_1m_2\bar{\omega}_1^2\bar{\omega}_2^2)^{3/2}}{[2\pi k_B(m_1\bar{\omega}_1^2T_2 + m_2\bar{\omega}_2^2T_1)]^{3/2}}, \quad (3)$$

with N_1 (N_2) the number of atoms of component 1 (2).

- [67] C. R. Monroe, E. A. Cornell, C. A. Sackett, C. J. Myatt, and C. E. Wieman, *Phys. Rev. Lett.* **70**, 414 (1993).